Langmuir **2007,** *23,* 9505−9512

Electroosmotic Flow in a Microcavity with Nonuniform Surface Charges

David Halpern[†] and Hsien-Hung Wei*[,‡]

Department of Mathematics, University of Alabama, and Department of Chemical Engineering, National Cheng Kung University, Tainan 701, Taiwan

Received May 9, 2007. In Final Form: June 12, 2007

In this work, we theoretically explore the characteristics of electroosmostic flow (EOF) in a microcavity with nonuniform surface charges. It is well known that a uniformly charged EOF does not give rise to flow separation because of its irrotational nature, as opposed to the classical problem of viscous flow past a cavity. However, if the cavity walls bear nonuniform surface charges, then the similitude between electric and flow fields breaks down, leading to the generation of vorticity in the cavity. Because this vorticity must necessarily diffuse into the exterior region that possesses a zero vorticity set by a uniform EOF, a new flow structure emerges. Assuming Stokes flow, we employ a boundary element method to explore how a nonuniform charge distribution along the cavity surface affects the flow structure. The results show that the stream can be susceptible to flow separation and exhibits a variety of flow structures, depending on the distributions of zeta potentials and the aspect ratio of the cavity. The interactions between patterned EOF vortices and Moffatt eddies are further demonstrated for deep cavities. This work not only has implications for electrokinetic flow induced by surface imperfections but also provides optimal strategies for achieving effective mixing in microgrooves.

1. Introduction

Thanks to the recent advance of micro/nanotechnology, parallel processing and automation on a small scale are now possible and have provided new paradigms for fulfilling various functions in an integrated, miniaturized device under the theme of microfluidics. Because fluid/mass transport processes such as pumping, mixing, and separation are indispensable to almost every microchip-based analysis, the key to successfully realizing desired operations often relies on the ability to control and manipulate the underlying transport processes. Although considerable efforts have been made toward this aim, electrokinetics actuation has recently emerged as a promising means to transport analytes on a small scale because it can be achieved on a portable device with embedded microelectrodes and, more importantly, it offers a diversity of manipulation capabilities without moving parts.

The most common way to convey fluids using electrokinetic effects is through electroosmostic flow (EOF). The phenomenon arises from the movement of space charges under the action of an applied electric field. Because these charges (mostly counterions) are typically bound to the surface within a thin (10−100 nm) electric double layer, they create large surface fields and establish Poisson−Boltzmann equilibrium instantly ($\sim 10^{-7}$ s) across the layer. This short-range surface charge effect immediately allows the double layer to screen external fields normally, making the double layer act like an insulator. Because this thin charge cloud acts as a mobile "sheath" next to the surface and can migrate only *tangentially* in response to an applied field, its motion in turn drags the adjacent fluid through the effect of viscosity, and the resulting fluid motion will look as if the surface is sliding. This creates an EOF with a characteristic Smoluchowski velocity[1]

$$U = -\frac{\epsilon \zeta^* E}{\mu} \tag{1}$$

where ϵ and μ stand for the permittivity and viscosity of the fluid, respectively, ζ^* is the surface zeta potential across the double layer, and E is the applied tangential field along the surface.

Because EOF appears as a macroscopic slip flow and is independent of the channel width d, it looks like a plug flow and hence eliminates significant Taylor dispersion commonly encountered in hydrodynamic pressure-driven flow. Because the flow rate is now proportional to d^2, EOF has a smaller flow resistance than pressure-driven flow (whose velocity scale and flow rate are proportional to d^2 and d^4, respectively). In addition, because much stronger electric fields can be rendered on small length scales, EOF is more effective for transporting fluids than for pressure-driven flow in microdevices.

Although EOF appears to be advantageous to transport fluids on a small scale, a *pure* EOF on uniformly charged surfaces often suffers from mixing deficiencies and lacks other manipulation abilities (e.g., the trapping of particles) because its irrotational nature does not permit vortices or recirculating streaming necessary for these processes. One way to overcome these shortcomings is to impose nonuniform charges on the surfaces. Because the analogy between electrostatics and hydrodynamics now breaks down, this in turn provides an alternative route to creating vortices needed for engineering the flow. Anderson and Idol[2] first demonstrated this idea and found secondary flows in a capillary with axial variation in the surface zeta potential. Ajdari[3] later showed a variety of recirculating EOF structures through spatial modulation of the surface charge densities of the channel walls. Stroock et al.[4] experimentally investigated EOF with charge-patterned strips and verified the existence of recirculating flow structures predicted by theory. As such, the concept of patterned EOF can indeed be realized and justified.

---

* Corresponding author. E-mail: hhwei@mail.ncku.edu.tw.

[†] University of Alabama.

[‡] National Cheng Kung University.

[1] Probstein, R. F. *Physicochemical Hydrodynamics: An Introduction*; Wiley-Interscience: Hoboken, NJ, 2003.

[2] Anderson, J. L.; Idol, W. K. *Chem. Eng. Commun.* **1985**, *38*, 93−106.

[3] Ajdari, A. *Phys. Rev. Lett.* **1995**, *75*, 755−758.

[4] Stroock, A. D.; Weck, M.; Chiu, D. T.; Huck, W. T. S.; Kenis, P. J. A.; Ismagilov, R. F.; Whitesides, G. M. *Phys. Rev. Lett.* **2000**, *84*, 3314−3317.

10.1021/la701343s CCC: $37.00

The ideas of utilizing patterned EOF have been explored in various microfluidic manipulations. By making use of time periodic alternations of zeta potentials[5] or surface patterning,[6] one can generate chaotic advection or 3D flow structures to enhance mixing. An EOF with obliquely patterned surface charges in a straight microchannel has also been shown to be capable of generating significant swirling/secondary flows for mixing.[7] Strategies using patterned EOF are also developed for designing micropumps through asymmetric channels or electrode designs under ac fields.[3,8] It could also have the potential to stretch or trap macromolecules.[9] A patterned EOF can further work with another imposed flow (e.g., pressure-driven flow) and yield a variety of flow structures (e.g., closed streamlines or even saddle points), depending on the relative flow strength.[10] Judicious control of these flows might fulfill a variety of particle manipulations (e.g., mixing, trapping, separation, etc). A recent study[11] with a cross-slot channel design demonstrated that nontrivial interactions between a patterned EOF and electrophoresis can result in various types of motion of charged colloids, which further extends the ability to manipulate colloidal suspensions.

Although nonuniformly charged EOF has revealed rich flow features, most efforts are based on simple straight-channel geometry. In microfluidic or MEMS applications, however, a featured device, which often comprises of composite materials or a number of different layers, could display structures (e.g., grooves or slits) with nonuniform depths in the channel geometry. If there is any defect, for example, due to imperfect coating or etching, nonuniform charges could be exposed on the uneven surfaces and hence be susceptible to EOF vortices in the presence of electric fields, which could be undesirable if dispersion is critical to the process. However, the mixing of analytes or the performance of precise manipulations in such a device using pure EOF would be unattainable unless one imposes nonuniform surface charges or other electrokinetic effects are included.[12]

Motivated by the above, it seems that there is a need to understand how non-straight-channel geometry affects the structures of nonuniformly charged EOF. There are two effects arising from non-straight geometries. First, the electric field is no longer uniform, as it must be larger (smaller) in a narrower (wider) cross section according to Gauss's law. It thus follows that the Smoluchowski velocities are not all the same along the channel surfaces even with the same surface charge. If the walls are charge patterned, then this electric field can produce EOF recirculating patterns that are qualitatively different from those in the straight-channel case. Second, the flow field can be further mediated by geometric effects due to a nonuniform cross-sectional area. Because the fluid must fulfill the requirement of a constant flow rate across the channel, this effect inevitably causes adverse pressure gradients and hence affects the flow structure because of the suppression or extension of the patterned EOF rolls.[10]

There have been only a few attempts to understand the EOFs in nonstraight geometries with nonuniform surface charges. Qian and Bau[13] studied the EOF in a closed cavity whose top and bottom walls have different surface charges and are subjected to a uniform electric field generated by sidewall electrodes. They solved the flow analytically and demonstrated a variety of recirculating flow patterns, depending on the distributions of the surface charges. Furthermore, they modulated these flows alternatively to create chaotic mixing in which a blob of nondiffusive tracers can undergo rapid folding and unfolding as a result of the temporal change of the flow structure. Hahm et al.[14] recently carried out simulations to study electrokinetic flow in a grooved microchannel having patterned charges on its side surfaces. In their model, the top and bottom surfaces of the channel are electrodes, which are able to generate an electric field that acts vertically across the groove. The resulting flow again exhibited various streamline patterns, depending on the surface charges of the side surfaces and the interaction between hydrodynamic flow and EOF. They also explored solute transport using these flows and demonstrated the ability to control the behavior of the transport.

In this work, we examine the flow behavior of EOF in an open microcavity with nonuniform surface charges. Recall that a uniformly charged EOF does not permit any flow separation because of its irrotational nature, yet an EOF with nonuniform surface charges will render vorticity. It is therefore our intent to examine its susceptibility to flow separation as compared to the classical benchmark problem, viz., viscous flow through a no-slip cavity. Because the latter case often accompanies the formation of Moffatt eddies,[15] it is also interesting to determine if an EOF in a nonuniformly charged cavity will bear similar features due to nontrivial vorticity generation. More importantly, interactions between patterned EOF vortex and Moffatt eddies could exist, which will also be explored in the present study. The article is organized as follows. We formulate the problem in section 2. The solution method is provided in section 3. Various flow structures will be presented and discussed in section 4. In section 5, comparisons are made between the present work and previous studies. Conclusions are given in section 6.

2. Problem Formulation: Geometry, Governing Equations, and Boundary Conditions

In this work, we consider 2D steady electroosmotic flow inside a rectangular cavity of width W and depth D. The upper corners of the cavity are rounded to avoid singularities in the electric and flow fields. The effect of having rounded corners will be discussed in the next section. Cartesian coordinates (x^*, y^*), with the origin defined at the center on the upper-surface plane, are used to describe the geometry, with the side walls of the cavity defined at $x^* = \pm W/2$ for $-D \leq y^* \leq -\delta D$ where $\delta D \ll D$ is the radius of the rounded corner and the bottom wall defined at $y^* = -D$ for $|x^*| \leq W/2$.

Here we are interested only in the region outside the thin double layer in which the solution remains electroneutral (the Ohmic region). Writing the electric field $\mathbf{E}^* = -\nabla\phi^*$ in terms of the electric potential ϕ^*, Gauss's law demands that the field in the Ohmic region must satisfy the Laplace equation:

$$\nabla^{*2}\phi^* = 0 \qquad (2)$$

Because double-layer screening does not permit normal penetration from the external field, it furnishes the insulating boundary condition at the boundaries

---

[5] Qian, S. Z.; Bau, H. H. *Anal. Chem.* **2002**, *74*, 3616−3625.
[6] Biddiss, E.; Erickson, D.; Li, D. *Anal. Chem.* **2004**, *76*, 3208−3213.
[7] Chang, C. C.; Yang, R. J. *J. Micromech. Microeng.* **2006**, *16*, 1453−1462.
[8] Ajdari, A. *Phys. Rev. E* **2000**, *61*, R45−48.
[9] Panwar, A. S.; Kumar, S. *J. Chem. Phys.* **2003**, *118*, 925−936.
[10] Wei, H. H. *J. Colloid Interface Sci.* **2005**, *284*, 742−752.
[11] Juang, Y. J.; Hu, X.; Wang, S. N.; Lee, L. J.; Lu, C. M.; Guan, J. J. *Appl. Phys. Lett.* **2005**, *87*, 244105.
[12] Hu, X.; Wang, S. N.; Juang, Y. J.; Lee, L. J. *Appl. Phys. Lett.* **2006**, *89*, 084101.
[13] Qian, S. Z.; Bau, H. H. *Appl. Math. Modell.* **2005**, *29*, 726−753.
[14] Hahm, J.; Balasubramanian, A.; Beskok, A. *Phys. Fluids* **2007**, *19*, 013601.
[15] Moffatt, H. K. *J. Fluid Mech.* **1964**, *18*, 1−18.

$$\mathbf{n}\cdot\nabla^*\phi^* = 0 \tag{3}$$

where $\mathbf{n}$ is the unit normal vector to the surface (pointing toward the liquid). Far away from the cavity, the field is uniform, $\mathbf{E}^* \rightarrow (E^*_\infty, 0)$ as $|\mathbf{x}^*| \rightarrow \infty$, which is rewritten as

$$\phi^* \rightarrow -E^*_\infty\, \mathbf{x}^* \text{ as } |\mathbf{x}^*| \rightarrow \infty \tag{4}$$

The motion of the electrolyte is governed by the Stokes and continuity equations

$$\nabla^* p^* = \mu \nabla^{*2}\mathbf{u}^*, \qquad \nabla^*\cdot\mathbf{u}^* = 0 \tag{5}$$

where $\mathbf{u}^* = (u^*, v^*)$ is the fluid velocity with horizontal and vertical components u^* and v^*, and p^* is the fluid pressure. The flow is driven by the slip walls subject to eq 1

$$\mathbf{u}^* = \frac{\epsilon}{\mu}\zeta^*(\mathbf{x}^*)\ \nabla^*\phi^* \tag{6}$$

with different zeta potentials at the walls

$$\zeta^* = \begin{cases} \zeta^*_\infty \text{ on AB and EF;} \\ \frac{1}{2}(\zeta^*_\infty + \zeta^*_{\mathrm{s}} + [\zeta^*_\infty - \zeta^*_{\mathrm{s}}]\cos 2\theta) \text{ on} \\ \quad \text{BB}'(-\pi \le \theta \le -{}^{\pi}/_{2}) \text{ and E}'\text{E}(-{}^{\pi}/_{2} \le \theta \le 0); \\ \zeta^*_{\mathrm{s}} \text{ on B}'\text{C and DE}'; \\ \zeta^*_{\mathrm{b}} \text{ on CD} \end{cases} \tag{7}$$

where the sides of the cavity AB, BB′, B′C, CD, DE′, E′E, and EF are as shown in Figure 1 and θ is the angle between the x axis and the cavity wall. Here we assume that $\zeta^*_\infty > 0$ for the flat surface outside the cavity, so EOF sufficiently far away from the cavity is subjected to a uniform flow

$$\mathbf{u} \rightarrow (-U_\infty, 0) \text{ as } |\mathbf{x}^*| \rightarrow \infty \tag{8}$$

where $U_\infty = \epsilon\zeta^*_\infty E^*_\infty/\mu$ is the Smoluchowski velocity scale. We nondimensionalize the problem by normalizing the following quantities:

$$x = \frac{x^*}{W},\ y = \frac{y^*}{W},\ \mathbf{u} = \frac{\mathbf{u}^*}{U_\infty},\ p = \frac{p^*}{(\mu U_\infty/W)},\ \mathbf{E} = \frac{\mathbf{E}^*}{E^*_\infty},\ \zeta = \frac{\zeta^*}{\zeta^*_\infty} \tag{9}$$

Hereafter, we will solve the following dimensionless governing equations and boundary conditions and discuss the results that follow:

$$\nabla^2\phi = 0, \qquad \nabla p = \nabla^2\mathbf{u}, \qquad \nabla\cdot\mathbf{u} = 0 \tag{10}$$

$$\mathbf{n}\cdot\nabla\phi = 0, \qquad \mathbf{u} = \zeta\nabla\phi \text{ on the boundary ABB}'\text{CDE}'\text{EF} \tag{11}$$

$$\phi \rightarrow -x,\ \mathbf{u} \rightarrow (-1, 0) \text{ as } |\mathbf{x}| \rightarrow \infty \quad \text{(along AA}', \text{FF}', \text{and A}'\text{F}') \tag{12}$$

3. Boundary Integral Methods for Solving Electric and Flow Fields

We employ boundary integral methods to solve numerically for the electric potential distribution and EOF field. As shown in Figure 1, the domain includes the rectangular cavity and the far field (AA′, FF′, and A′F′) where both the electric and velocity fields are set to be uniform.

By applying Green's theorem to the Laplace equation for the electric potential (eq 2), we obtain the following integral equation for ϕ and the normal gradient $\partial\phi/\partial n$ along surface S, the boundary of the computational domain shown in Figure 1

$$C\phi(\mathbf{x}) + \int_S \phi(\mathbf{y})\frac{\partial G}{\partial n}\,\mathrm{d}S(\mathbf{y}) = \int_S \frac{\partial\phi}{\partial n}(\mathbf{y})\ G(\mathbf{x}, \mathbf{y})\ \mathrm{d}S(\mathbf{y}) \tag{13}$$

where $G(\mathbf{x}, \mathbf{y}) = -{}^{1}/_{2\pi} \log(|\mathbf{x} - \mathbf{y}|)$ is the free-space Green function and $C = {}^{1}/_{2}$ if $\mathbf{x}$ is on the boundary but $C = 0$ otherwise. As for the flow field, the Stokes equation (eqs 5) are also solved in a similar fashion, yielding the following integral equation linking the velocity and the stress on the domain S

$$C_{ki}u_i(\mathbf{x}) + \int_S T_{ik}(\mathbf{x}, \mathbf{y})\ u_i(\mathbf{y})\ \mathrm{d}S(\mathbf{y}) = \int_S U_{ik}(\mathbf{x}, \mathbf{y})\ \tau_i(\mathbf{y})\ \mathrm{d}S(\mathbf{y}) \tag{14}$$

where $\mathbf{x}$ is a point on surface S, $\tau = \sigma\mathbf{n}$ is the stress vector, C_{ki} is a tensor that allows for a jump in normal stress, and U_{ik} and T_{ik} are kernels based on the free-space Green function:

$$U_{ik} = -\frac{1}{4\pi}\left(\delta_{ik}\log\left|\mathbf{x} - \mathbf{y}\right| - \frac{(x_i - y_i)(x_k - y_k)}{|\mathbf{x} - \mathbf{y}|^2}\right)$$

$$T_{ik} = -\frac{1}{\pi}\,\frac{(x_i - y_i)(x_j - y_j)(x_k - y_k)n_j(\mathbf{y})}{|\mathbf{x} - \mathbf{y}|^4} \tag{15}$$

We apply the boundary element method[16,17] to determine ϕ, $\partial\phi/\partial n$, $\mathbf{u}$, and τ on S and within the cavity. Domain S is discretized into N quadratic elements, each having three nodes. Along each element, ϕ, $\partial\phi/\partial n$, $\mathbf{u}$, and τ are approximated using quadratic polynomials and expressed in terms of a local arclength coordinate. The potential ϕ and the velocity field $\mathbf{u}$ are assumed to be continuous everywhere. To ensure this at the upper rounded corners of the cavity, the zeta potential ζ is allowed to vary smoothly from its prescribed value outside the cavity, $\zeta = 1$, to its prescribed value along the side walls of the cavity, $\zeta = \zeta_{\mathrm{s}}$, according to the dimensionless form of eq 7. Two systems of linear equations are then obtained, one for the unknown ϕ or $\partial\phi/\partial n$ along each of the boundaries that comprise S and the other for either $\mathbf{u}$ or τ

$$H_\phi\phi = G_\phi\frac{\partial\phi}{\partial n}, \qquad H_{\mathrm{u}}\mathbf{u} = G_{\mathrm{u}}\tau \tag{16}$$

where H_ϕ, G_ϕ, H_{u}, and G_{u} are respectively $2N \times 2N$, $3N \times 3N$, $4N \times 4N$, and $6N \times 6N$ matrices whose elements are computed using Gaussian quadrature rules. These matrices are solved using Gaussian elimination with partial pivoting for the unknown ϕ, $\partial\phi/\partial n$, $\mathbf{u}$, and τ along S. The electric and velocity fields within the cavity can then be readily computed from eqs 13 and 14 by choosing the appropriate values for the scalar C and tensor C_{ki}.

Care must be taken concerning the numerical simulation of the electric field. It is well known from classical electrostatic theory that there is a singularity of the electric field at a corner if the wedge angle θ (measured on the fluid side) is greater than π, as analogous to theory for potential flow.[18] Namely, the local electric field in the neighborhood of the corner is identified as $E \propto r^{(\pi/\theta) - 1}$ and so is the corresponding slip EOF velocity, where r is the distance from the corner. Therefore, singularities occur at the upper corners of the cavity if the unit normal vector

---

(16) Brebbia, C. A.; Dominguez, J. *Boundary Elements: An Introductory Course*; McGraw-Hill: New York, 1992.

(17) Pozrikidis, C. *Boundary Integral and Singularity Methods for Linearized Viscous Flow*; Cambridge University Press: Cambridge, U.K., 1992.

(18) Batchelor, G. K. *An Introduction to Fluid Dynamics*; Cambridge University Press: Cambridge, UK, 1967.

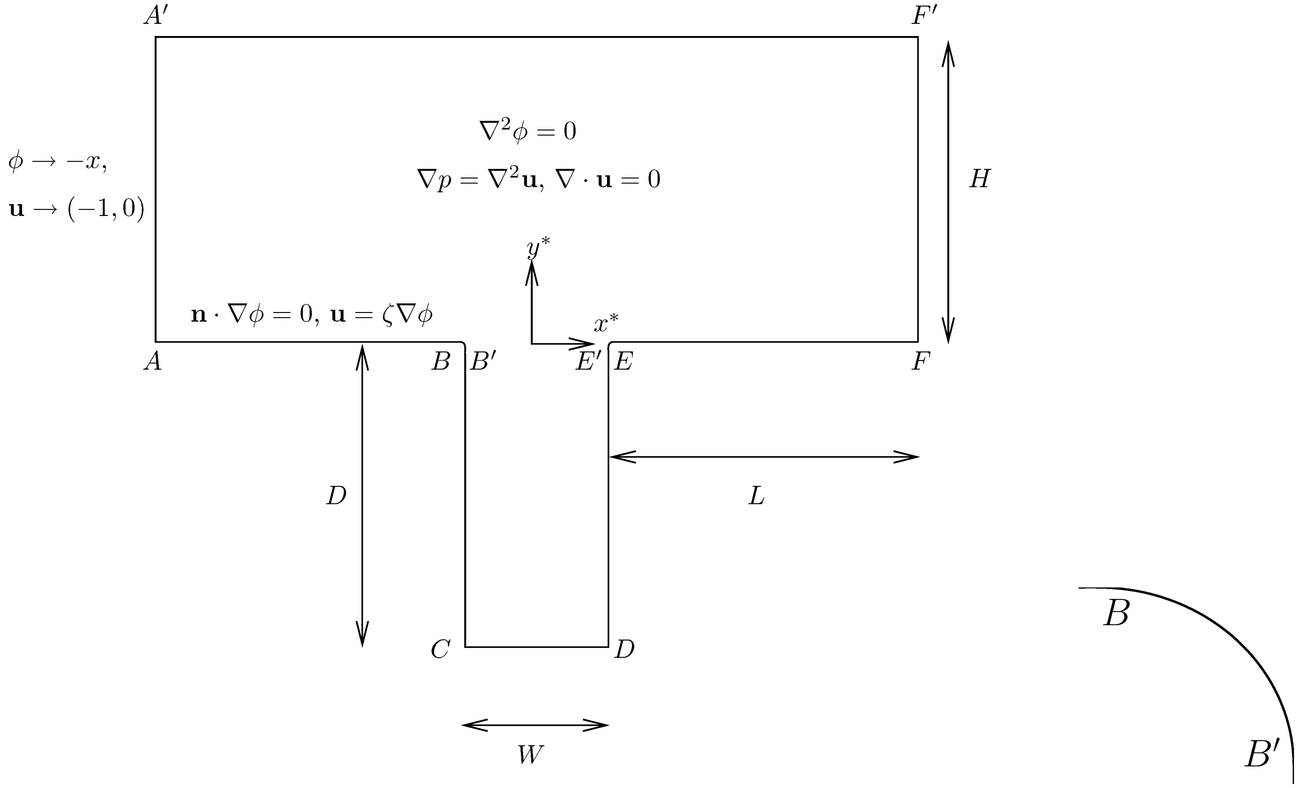

Figure 1. Computational domain used to solve for flow and electric fields inside a 2D rectangular cavity of width *W* and depth *D*. Here, *L* and *H* are chosen to be sufficiently large so that the far-field conditions are applied along edges AA′, FF′, and A′F′. The right panel shows an enlarged view of the upper left corner of the cavity.

changes abruptly at these locations (from pointing horizontally/vertically just inside/outside the cavity). Fortunately, the singularities in fact manifest themselves only over the length scale on the order of the double layer near the corners. Also, as long as the wall's permittivity is sufficiently small compared to the fluid's,[19] field penetration across the corner could be weak and the effect could thus be considered only local; the field at a distance sufficiently far away from the corners is regular. Besides, a practical microdevice hardly has perfectly sharp edges. In view of the above, we circumvent the singularity problem by making the upper corners rounded so that the potential and velocity fields are continuous everywhere. Also, we choose the radius of curvature, δ, of these corners to be sufficiently small compared to macroscopic length scales so that the results do not vary with δ significantly. Here we use $\delta = 0.03$ throughout the simulations.

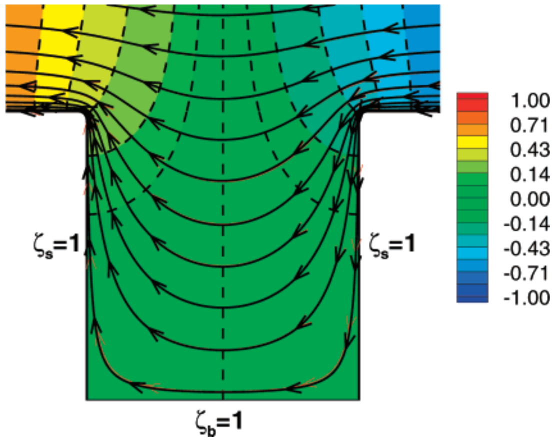

Figure 2. Streamlines (solid lines), electric field lines (red lines), and lines of constant electric potential (dashed lines) inside a square cavity for the case where $\zeta = 1$ on all surfaces. The color scale indicates the electric potential distribution. In this case, the flow is irrotational, and streamlines and electric field lines coincide.

4. Flow Characterization of Electroosmotic Flow in a Charged Patterned Cavity

The problem depends on the following parameters: the depth to width ratio D/W, the zeta potential along the two vertical side walls, ζ_s, and the zeta potential along the bottom wall of the cavity, ζ_b. Outside the cavity, $\zeta = 1$. First, we test the simplest case: a square cavity ($D/W = 1$) having a uniform zeta potential everywhere along the boundaries. Figure 2 shows the resulting electric field and streamlines. Here the dashed lines correspond to isopotential contours that must be perpendicular to the electric field lines. This result clearly shows that the electric field lines and streamlines coincide as a consequence of the electrostatics−hydrodynamics similitude. Because the flow is proved to be irrotational, neither flow separation nor vortex formation occurs in this case. Increasing the depth of the cavity, no matter how deep, does not give rise to any flow separation because of the irrotational nature of this flow. This feature could be advantageous for transporting fluids into deep grooves with high aspect ratios, as opposed to pure hydrodynamics-driven flow in which Moffatt eddies are often present within the cavity and hence significantly reduce flow penetration depth.

Figure 3 shows the case in which we place no surface charge on the cavity walls (i.e., $\zeta_s = \zeta_b = 0$). This case can be thought as uniform flow past a no-slip cavity. The cavity wall now serves as a source of vorticity because there must exist substantial velocity gradients on the no-slip wall. Meanwhile, an adverse pressure gradient must develop to counterbalance the viscous force within the cavity in order to fulfill the requirement of constant flow rate across the depth. As a result, the flow exhibits a large counterclockwise circulating eddy within the cavity.

---

[19] Thamida, S. K.; Chang, H.-C. *Phys. Fluids* **2002**, *14*, 4315−4328.

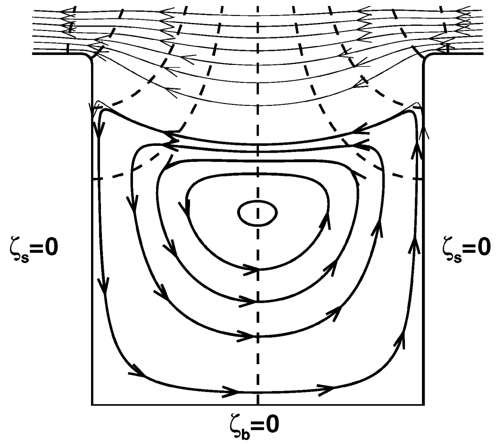

Figure 3. Uniform flow outside the cavity drives a large counterclockwise circulating eddy within the cavity whose walls are no-slip because of zero surface charge. For the bottom vortex, $\Delta\psi = 0.00225$, and above it, $\Delta\psi = 0.02$. Here, $\Delta\psi$ stands for the interval of the stream function values.

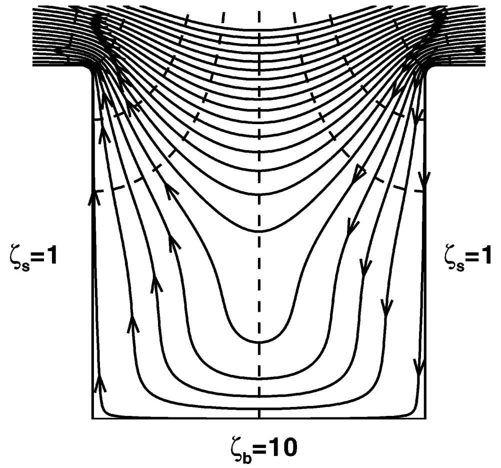

Figure 4. Effect of the bottom zeta potential ζ_b on the flow structure. For small and moderate values of ζ_b, the flow simply enters and leaves the cavity without eddies. Here, the interval of the stream function values is $\Delta\psi = 0.013$.

We now consider the effect of increasing the zeta potential along the bottom wall but retaining $\zeta_s = 1$ along the sides of the cavity. Here we set the slip velocity at the bottom wall to be in the same direction as the free stream. Because the electric field attenuates rapidly as it penetrates the cavity, for small and moderate values of ζ_b the bottom-wall velocity is generally no faster than the free-stream velocity. In this case, the fluid simply enters and then leaves the cavity, as depicted in Figure 4.

However, when the velocity along the bottom wall exceeds the free-stream velocity at some critical value of ζ_b (i.e., $\zeta_b^* \approx 12.5$), this causes the streamlines at the bottom to turn clockwise, giving rise to a small vortex and the appearance of a saddle point within the cavity, as shown in Figure 5. This vortex grows in size when ζ_s is decreased (Figure 6), which is attributed to the lack of lateral suppression from the slip flow set by the side walls.

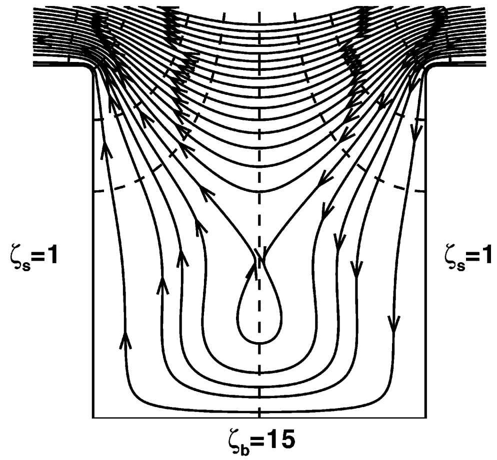

Figure 5. Saddle point appearing in the flow with a small vortex if the bottom zeta potential exceeds some critical value. Here, the interval of the stream function values is $\Delta\psi = 0.01235$.

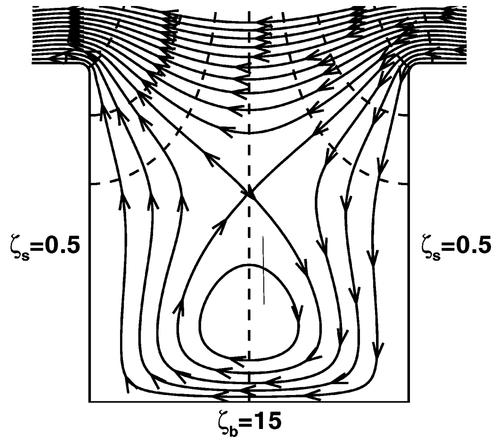

Figure 6. As compared to Figure 5, the vortex in the cavity grows in size as the bottom zeta potential decreases. Here, the interval of the stream function values is $\Delta\psi = 0.01185$.

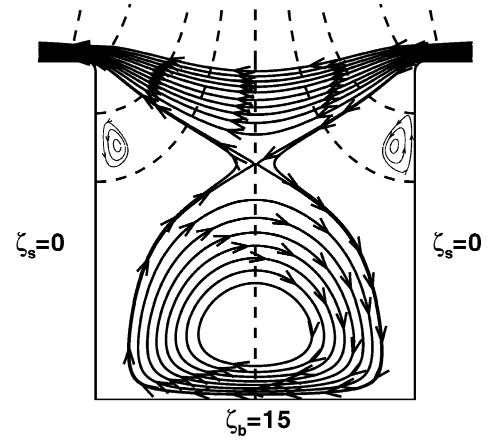

Figure 7. Streamlines for the case where no-slip is applied along the side walls of the cavity. The flow field consists of a large eddy rotating in a clockwise manner and two small counterclockwise vortices near the top of the cavity. For the small vortices, $\Delta\psi = 6.3 \times 10^{-5}$; otherwise, $\Delta\psi = 0.0057$. Here, $\Delta\psi$ stands for the interval of the stream function values.

When $\zeta_s$vanishes, the clockwise vortex virtually fills the whole cavity, as shown in Figure 7. In addition, there are two counterclockwise microvortices formed between the saddle point and the side walls. Such peculiar flow behavior can be explained below. Whereas the free stream (toward the left) and the primary vortex (in a clockwise direction) must join at the saddle point, the streamlines that separate these flows create "wedges" between themselves and the side walls, making the fluid in effect confined within the wedges. Because the streams along the two sides of each wedge follow the same direction and the nearby no-slip side wall tends to retard the flow, a vortex must develop in this confined region as a result of fluid mass conservation.

If we now decrease the zeta potential ζ_b on the bottom wall for Figure 7, a new flow feature emerges, as shown in Figure

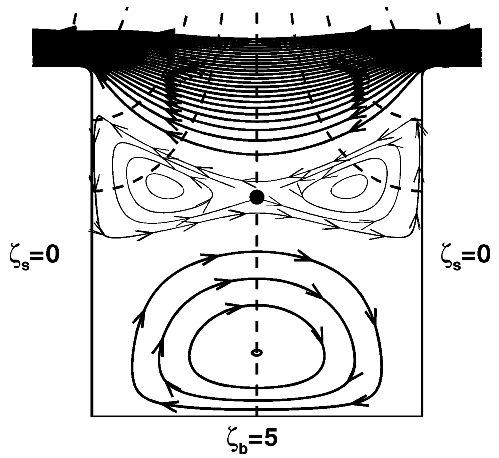

Figure 8. As compared to Figure 7, a reduction in the zeta potential of the bottom wall results in a small vortex near the bottom wall and the coalescence of the two smaller vortices near the top of the cavity. The circular marker denotes the location of the saddle point. For the bottom vortex and the streamlines near the entrance to the cavity, $\Delta\psi = 0.005$, and for the streamlines in the vicinity of the saddle point, $\Delta\psi = 0.0006$. Here, $\Delta\psi$ stands for the interval of the stream function values.

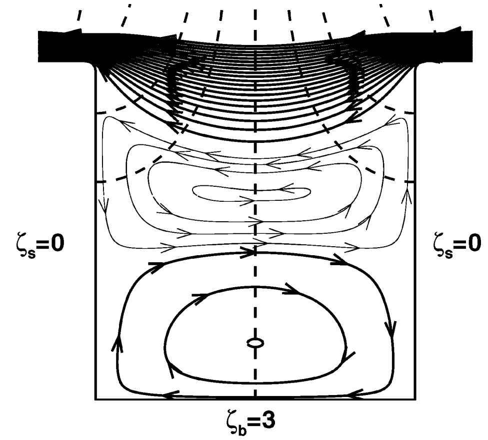

Figure 9. Decreasing size of the vortex near the bottom of the cavity with decreasing ζ_b. At the same time, the second vortex in the upper portion of the cavity grows in size and eventually suppresses the bottom one as $\zeta_b \to 0$ (Figure 3). For the bottom vortex and the streamlines near the entrance to the cavity, $\Delta\psi = 0.005$, and for the middle vortex, $\Delta\psi = 0.0012$. Here, $\Delta\psi$ stands for the interval of the stream function values.

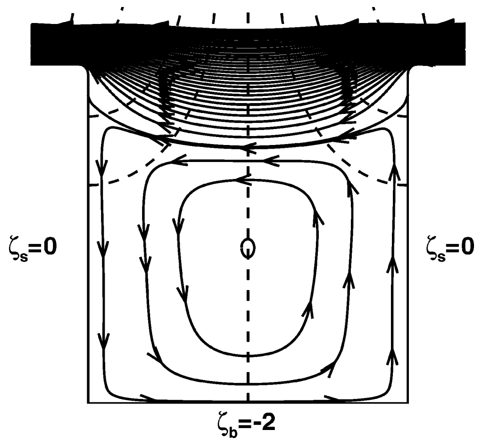

Figure 10. Single counterclockwise-rotating eddy filling the whole cavity for the case where $\zeta_b < 0$ and no-slip is applied along the side walls, $\zeta_s = 0$. Here, the interval between the stream function values is $\Delta\psi = 0.0045$.

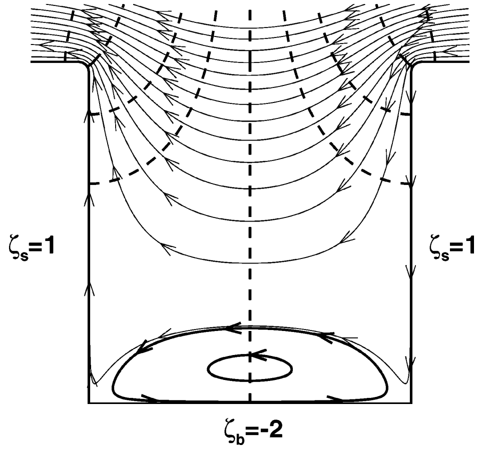

Figure 11. Eddy close to the bottom wall shrinks in size if there is some slip along the side walls, $\zeta_s = 1$. The external flow effectively sees a shallower cavity. $\Delta\psi = 0.004$ for the bottom vortex, and $\Delta\psi = 0.02$ above it. Here, $\Delta\psi$ stands for the interval of the stream function values.

8. Although the central primary eddy diminishes in size (because of the decreased driving velocity set at the bottom wall), the two smaller vortices are now encompassed by one larger counterclockwise rotating roll but are separated by a saddle point in between. As ζ_b is further decreased, these two smaller vortices merge, forming a larger counterclockwise roll in the upper portion of the cavity (Figure 9). As $\zeta_b \to 0$, the counterclockwise roll eventually suppresses the bottom vortex as shown in Figure 3.

The results shown above are for the case in which the surface charge on the bottom cavity is the same sign as that on the exterior surface; that is, the slip motion on the bottom wall is in the same direction as the free stream. We now examine the $\zeta_b < 0$ scenario where the bottom-wall slip motion is in the opposite direction to the free stream velocity. If there is no surface charge on the side walls, then a counterclockwise circulating vortex must develop in the cavity (Figure 10), which can be thought of as a flow sandwiched by two oppositely moving lids.

However, if $\zeta_s \geq 1$, the slip side-wall flow, working together with the free stream, is able to suppress the vortex and hence confine it to the lower portion of the cavity, preventing the fluid from further penetrating the cavity (Figure 11). In this case, the external flow essentially sees a shallower cavity.

As shown above, we have identified a diversity of flow patterns arising from a variety of surface charge conditions inside the cavity. In particular, when the bottom surface charge is of the same sign as the exterior surface, the flow behavior can exhibit a simple in-and-out stream (Figure 4), various saddle-point flow structures (Figures 5−8), or two vortices (Figure 9). Because the changes between these flow characteristics for this case depend on whether the saddle point appears or disappears, we construct a flow map in Figure 12 to see how the flow structure changes from one surface charge condition to another.

For small ζ_s (<0.3), the critical ζ_b for the appearance of a saddle point (Figure 8) decreases with ζ_s because a small ζ_s causes the generation of vorticity on the side walls, which is prone to create a vortex in the top portion of the cavity. Because this side-wall vortex grows with decreasing ζ_s, the formation of a saddle point must entail a sufficiently large EOF roll to prevent the fusion of the two side-wall vortices, which requires a larger ζ_b. As ζ_s becomes larger (>0.3), the side walls become more slippery, and the resulting critical ζ_b increases with ζ_s. For large ζ_s, the fluid tends to enter and leave the cavity without the formation of vortices (Figure 4). In this case, the formation of

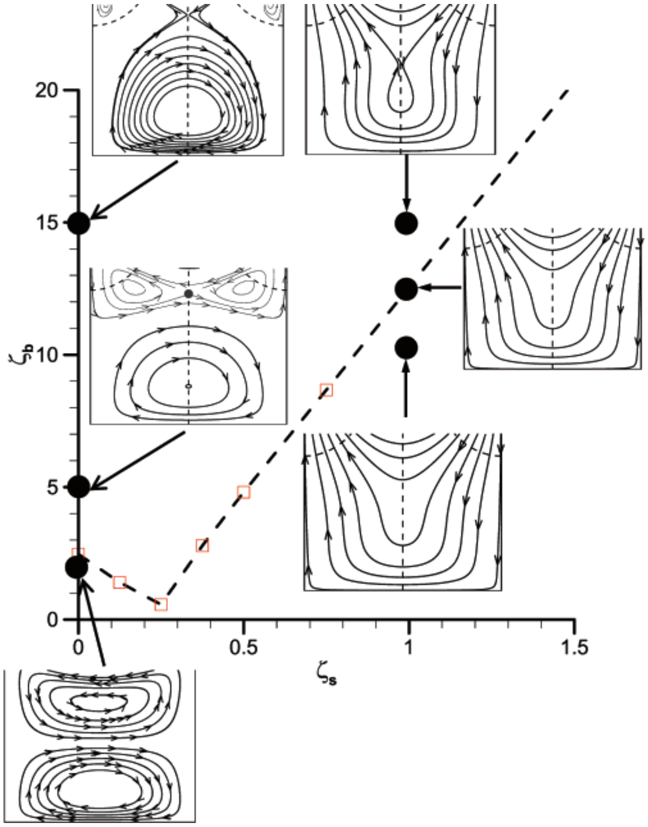

Figure 12. Line $\zeta_b^{crit}(\zeta_s)$ indicating the critical ζ_b value for the appearance of a saddle point in the flow field inside a square cavity.

a saddle point requires a sufficiently large mismatch between the free stream and the bottom slip velocities. In addition, the electric field at the bottom is weaker than that outside the cavity. Therefore, the bottom wall demands a larger surface charge to produce a sufficiently fast slip velocity to compete with the free stream so as to change the flow structure qualitatively.

After examining the flows in square cavities ($D/W = 1$), we now inspect a few cases to illustrate the effects of the aspect ratio D/W on the flow structure. We first examine $D/W > 1$, which corresponds to a deep cavity. Here, the primary focus is to explore the interaction between Moffatt eddies and patterned EOF rolls. To do this, we set the side walls to zero charge, which makes the side walls nonslip so that the flow is susceptible to the formation of Moffatt eddies inside the cavity. As a reference case, we first show streamlines within a no-slip cavity with $D/W = 3$ in Figure 13a and confirm the formation of Moffatt eddies. When the bottom zeta potential is positive and sufficiently large, we find two recirculating vortices with a saddle point—a combination of a Moffatt vortex in the upper cavity and an EOF-induced vortex near the bottom wall, as shown in Figure 13b. This is because, whereas a series of Moffatt eddies tends to develop along the depth of the cavity, the flow will be mediated by the EOF-induced vortex at the bottom. The adjustment between these two flow structures thus leads to the formation of a saddle point.

As for $D/W < 1$, which corresponds to a shallow cavity, Figure 14a−d shows various stream patterns for $D/W = 0.5$ with $\zeta_s = 0$. For $\zeta_b = 0$, the flow exhibits two vortices separated by a saddle point (Figure 14a). These vortices are suppressed and separated by increasing ζ_b (Figure 14b). At moderate ζ_b, the vortices vanish, and the flow turns into a simple in-and-out pattern (Figure 14c), as the bottom-wall slip velocity tends to assist the free-stream flow that attenuates when penetrating the cavity. At sufficiently large ζ_b, however, the free stream cannot match the flow created by the bottom wall. Hence, we find a saddle-point structure (Figure 14d).

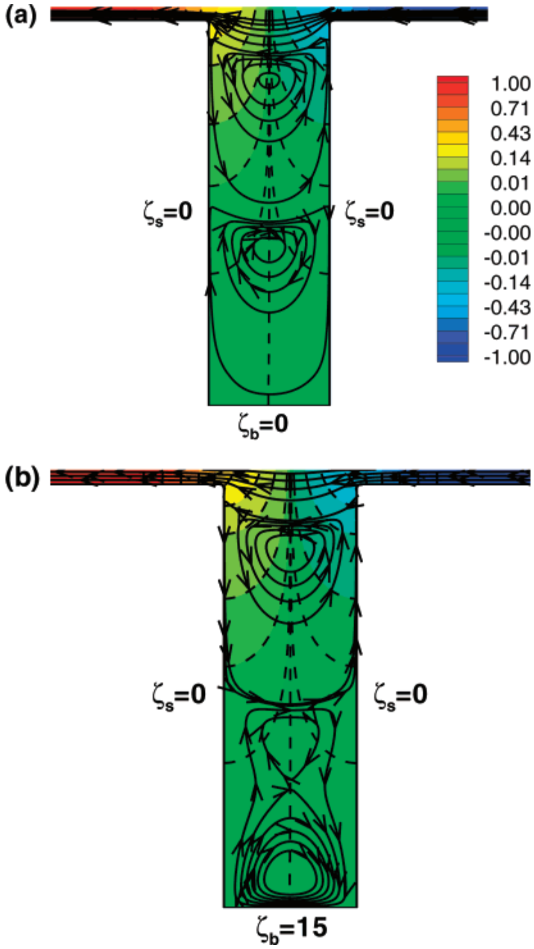

Figure 13. (a) Streamlines in a no-slip, deep cavity with an aspect ratio of $D/W = 3$. The result clearly shows two Moffatt eddies within the cavity. For the two vortices, $\Delta\psi = -6.24 \times 10^{-6}$ for the one near the bottom wall, and $\Delta\psi = 0.00235$ for the one near the entrance to the cavity. The color scale indicates the electric potential distribution. (b) For the same cavity as in part a but with a charged bottom wall instead, a saddle-point flow structure forms in the lower portion of the cavity as a result of the interaction between the Moffatt eddies and the EOF vortex. For the bottom vortex, $\Delta\psi = 1.03 \times 10^{-5}$, for the top vortex, $\Delta\psi = 0.002$, and near the entrance to the cavity, $\Delta\psi = 0.03$. Here, $\Delta\psi$ stands for the interval of the stream function values.

5. Comparison with Previous Studies

Although there are only a few reports[13,14] of EOFs within microcavities with nonuniform surface charges, it is worthwhile to compare our work with these studies. Note that our geometry and boundary conditions are different from theirs. So, the comparison is merely qualitative and is made through the observation of flow patterns. This also provides additional verification for our numerical simulations and the physics thereof.

We first compare our work with Qian and Bau's[13] in which the flow is confined within a closed cavity. For flow in an open cavity as considered in the present study, we set up the free stream as a uniform flow passing over the cavity, which can somewhat be thought to act like a sliding lid by analogy to a closed cavity. This can be seen by the observation that for a no-slip square cavity our benchmark recirculating flow shown in Figure 3 is similar to their Figure 7c. In addition, when the

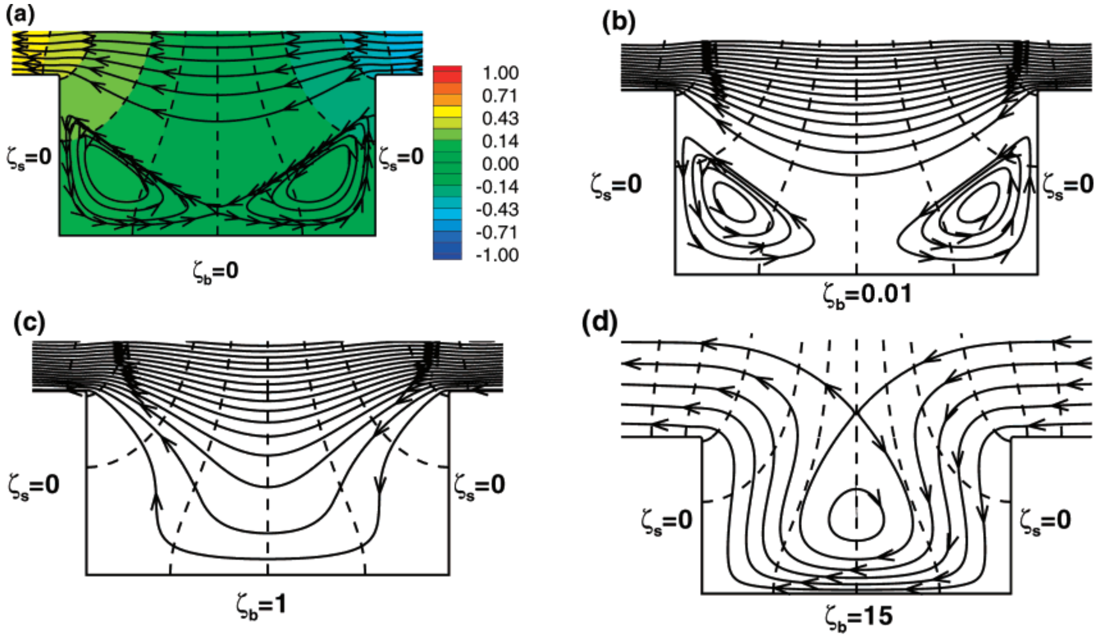

Figure 14. Effects of varying ζ_b on the flow structure inside a shallow cavity with $D/W = 0.5$ and $\zeta_s = 0$: (a) $\zeta_b = 0$. Near the entrance to the cavity, $\Delta\psi = 0.025$, and for the vortices in the cavity, $\Delta\psi = 2.5 \times 10^{-4}$. The color scale indicates the electric potential distribution. (b) $\zeta_b = 0.01$. Near the entrance, $\Delta\psi = 0.01$, and for the vortices, $\Delta\psi = 3 \times 10^{-4}$. (c) $\zeta_b = 1$ and $\Delta\psi = 0.01$. (d) $\zeta_b = 15$ and $\Delta\psi = 0.0708$. Here, $\Delta\psi$ stands for the interval of the stream function values.

bottom wall is charged and has a moderate slip velocity in the same direction as the free stream, we find in Figure 9 that two vortices are formed in a square cavity. This result is also in qualitative agreement with their Figure 7b,d for which the slip velocities of the top and bottom walls are in the same direction.

We also make comparisons with Hahm et al.,[14] who studied EOF in a grooved microchannel. As shown in our Figure 2 for the case with a uniformly charged surface, we identify that pure EOF is irrotational without flow separation. This result is virtually identical to that in their Figure 2b. For a no-slip cavity, our Figure 3 exhibits a single vortex, similar to that in their Figure 2a. If the surface charges are not uniform within the cavity, then the flow can exhibit vortices accompanied by the formation of saddle points, as shown in our Figures 5−8. This feature is qualitatively similar to those in their Figures 4 and 5.

6. Concluding Remarks

We have systematically investigated the flow character of EOF inside a microcavity with nonuniform surface charges. We have demonstrated that the flow exhibits a variety of patterns, depending on the surface charge distribution inside the cavity and the aspect ratio. Different flow structures are attributed to various interactions between the uniformly charged irrotational EOF free stream, Moffatt eddies generated from no-slip surfaces, and an EOF vortex created by patterned charged surfaces.

Our findings could have several implications in microfluidic applications. First, EOF vortices created by nonuniform surface charges will inevitably reduce the flow penetration depth in a cavity. This could be an undesirable effect for conveying solutes into the cavity. In other words, successful solute penetration must rely on the surfaces being uniformly charged to render the flow irrotational so as to eliminate these EOF vortices. Second, a surface defect or anomalous adsorption on the surfaces could cause nonuniform surface charges and hence generate undesired EOF patterns. Quite frequently, microfluidic applications involve geometric/surface patterning for specific purposes. Because the flow structure could be sensitive to the zeta potentials under certain geometric conditions (e.g., Figure 14), it is necessary to have adequate surface treatments in concert with geometric design to fulfill desired functions or to prevent unwanted dispersion.

Finally, a variety of recirculating flow patterns found in the present study obviously have the potential to create effective mixing. Because mixing must involve solutes crossing streamlines, if one employed an appropriate scheme (e.g., time periodic electric fields or zeta potentials) to change the flow pattern from one to another, it could be possible to create successive folding or unfolding of fluid elements for enhanced mixing.[5,10] In particular, because a flow pattern could exhibit a saddle-point flow structure that is dynamically unstable, one could even utilize such to create chaotic motion. This could provide an added advantage for creating mixing without appealing to complicated designs. Yet, it is worth noticing that although one could generate more complicated flow structures using a deep cavity to render mixing (e.g., Figure 13), the flow could be too sluggish to have noticeable convective effects. In this regard, optimization is needed in designing an efficient micromixer.

Acknowledgment. H.-H.W. acknowledges support by the National Science Council of Taiwan under grant NSC 95-2221-E006-310.

LA701343S